 doi:10.20944/preprints202105.0246.v1

Article

Early Identification of Root Rot Disease by Using Hyperspectral Reflectance: The Case of Pathosystem Grapevine/*Armillaria*

Federico Calamita [1,2*], Hafiz Ali Imran [1,3], Loris Vescovo [1], Mohamed Lamine Mekhalfi [5], and Nicola La Porta [1,4]

[1] Sustainable Ecosystems and Bioresources Department, Research and Innovation Centre, Fondazione Edmund Mach, Via E. Mach 1, 38098 San Michele all'Adige (TN), Italy; nicola.laporta@fmach.it (N.L.P.), loris.vescovo@fmach.it (L.V.)
[2] Metacortex S.r.l., Via dei Campi 27, Torcegno 38050, Italy
[3] Department of Civil, Environmental and Mechanical Engineering, University of Trento, Via Mesiano 77, 38123 Trento (TN), Italy; hafizali.imran@unitn.it (H.A.I.)
[4] EFI Project Centre on Mountain Forests MOUNTFOR, Via E. Mach 1, I-38098 San Michele All' Adige, TN, Italy.
[5] Department of Information Engineering and Computer Science, University of Trento, 38123 Trento, Italy; mohamed.mekhalfi@alumni.unitn.it (M.L.M).
* Correspondence: federico.calamita@alumni.unitn.it; Tel.: +39-3248759041

Abstract: The *Armillaria* genus represents one of the most common causes of chronic root rot disease in woody plants. The disease damage prompt assessment is crucial for pest management. However, the disease detection current methods are limited at the field scale. Therefore, an alternative approach that can enhance or supplement traditional techniques is needed. In this study, we investigated the potential of hyperspectral methods to identify the changes between fungi-infected and uninfected plants of *Vitis vinifera* in early detecting the *Armillaria* disease. The hyperspectral imaging sensor Specim-IQ was used to acquire images of leaves of the Teroldego Rotaliano grapevine cultivar. We analysed three groups of plants: healthy, asymptomatic, and diseased. Highly significant differences were found in the Near infrared (NIR) spectral region with a decreasing pattern from healthy to diseased plants attributable to internal leaf structure changes. Asymptomatic plants emerged from the other groups due to a smaller reflectance in the red-edge spectrum (around 705nm). Hypothetically associated with the presence of secondary metabolites involved in plant defence strategy. Furthermore, significant differences were observed in the wavelengths close to 550 nm in diseased plants versus asymptomatic. We used linear discriminant analysis from a machine learning context to classify the leaves based on the most significant variables (vegetation indices and single bands), with resulting overall accuracies of 85% and 84% respectively in healthy *vs*. diseased and healthy *vs*. asymptomatic. To our knowledge, this study represents the first report on the possibility of using hyperspectral data for root rot disease diagnosis on woody plants. Although further validation studies are required, it appears that the spectral reflectance technique, possibly implemented on unmanned aerial vehicles (UAV), could be a promising tool for a cost-effective, non-destructive method of *Armillaria* disease early diagnosis and mapping in the field, contributing to a significant step forward in precision viticulture.

Keywords: agriculture 4.0; chlorophyll; early diagnosis; fungal tree pathogens; mycology; plant disease; plant pathology; smart viticulture; vegetation indices; wine grapes.

1. Introduction

The *Armillaria* (Fr.: Fr.) Staude is a globally distributed and widely studied genus of pathogenic fungus belonging to the Basidiomycota class, Agaricales order, and Tricholomataceae family [1, 2]. It spreads under the soil through root contact or complex structures named rhizomorphs which can grow relatively fast for hundred meters and penetrate the roots bark of the hosts [3, 4]. A single individual of *Armillaria* was found in Michigan that occupied ca. 15 ha and weighed more than 10,000 kg [5] while in Oregon

Preprints (www.preprints.org) | NOT PEER-REVIEWED | Posted: 11 May 2021 doi:10.20944/preprints202105.0246.v1

another single individual was estimated growing over nearly 1,000 ha and as many as 8,650 years old, representing one of the largest and oldest living organisms on Earth [6]. *Armillaria spp*. are opportunistic parasites, however, some species, like *A. mellea* (Vahl) P. Kumm., are considered primary parasites of stressed trees [7] and are going to increase their damages under climate change conditions [8]. Besides, the modern context of agricultural intensification may offer an opportunity for *Armillaria* to adapt to single monocultures with a resulting disease grimness amplification [7]. Due to its saprophytic ability *Armillaria spp.* can feed on dead woody tissues after killing the host (e.g. stumps, roots, debris), and the mycelium can survive in woody residuals up to 15 or 20 years or more [9]. *Armillaria* spp. can parasitize a wide range of plant species in forest, both conifers and broadleaves [10], in garden trees and shrubs [11], and it can cause extensive losses in fruit orchards like apples and berries [12], pears [13], peaches [14, 15], kiwifruits [16], as well as grapevine [17–20].

1.1 Root symptoms

The host infection normally has a chronic course results in a rot collar and roots that lead to its death also after several years [7]. Roots appear dark, easily removable from the ground with a fibrous consistency [21, 22]. Furthermore, it is possible to perceive a strong scent of fresh mushrooms by smelling the roots, especially in humid conditions [23]. By scratching the collar and main roots bark with a small knife, it is possible to perceive a white mycelium that ends in the typical fan shape (**Error! Reference source not found.**). Dark brown rhizomorphs can be found in roots and soil. The presence of fruiting bodies is sporadic in the vineyard and could occur exclusively in autumn and after several years of infection [23].

Figure 1. Underground symptoms of *Armillaria* root rot in grapevine. Panel (a) shows the rotting wood and whitish mycelium in the subcortical area of the collar; panel (b) shows the fan mycelium in a detached fragment of collar cortex. Photo from the author, Mezzolombardo, TN, 24-08-2019.

1.2 Foliar symptoms

While the plant collars observation could be sufficient to obtain an accurate diagnosis [21], on the other hand, the disease is not easily ascribed from foliar symptoms themselves owing to their unspecificity. Additionally, foliar symptoms become visible when the diseased have reached an advanced stage and the host has been compromised [17]. According to Baumgartner et al. 2002, foliar symptoms do not appear until one-half to three-quarters of the main host root is colonized by *Armillaria mellea.* Aboveground *Armillaria* symptoms in grapevine include lower plant vigour and low fruit production with a generally suffering appearance, higher number of lateral shoots, dwarf and wilting leaves, stunted and not lignified shoots [17, 21, 23].

1.3 Disease diagnosis

Preprints (www.preprints.org) | NOT PEER-REVIEWED | Posted: 11 May 2021 doi:10.20944/preprints202105.0246.v1

Since there are no effective plant protection products in the market to control the pathogen [10], disease assessment is crucial for pest management. In fact, an accurate diagnosis in the field will improve the efficiency of prophylactic methods [7, 24], such as the prompt elimination of infected plants, root residuals removal, crop rotations, and the use of less susceptible rootstocks [19]. Traditionally, the disease damage assessment was estimated using a visual approach, relying upon direct observation in the vineyard. However, this method is time-consuming, labour-intensive, and costly for disease monitoring in large-scale farming. Consequently, there is a need to develop new approaches that can enhance or supplement traditional techniques. Additionally, early disease detection would increase the effectiveness of preventive measures typically used to face the pathogen. This study aims to investigate the potential of an alternative and non-destructive method to early detect root rot disease in grapevines.

1.4 The potential of hyperspectral sensors

Hyperspectral technology may represent a valuable alternative to traditional disease assessment and have proven to be a promising tool for disease diagnosis [25]. The use of hyperspectral sensors for crop disease assessment started many decades ago. In the early 1980s, Toler et al. used aerial colour infrared photography to evaluate root rot disease of cotton and wheat stem rust [26]. Reflectance data turned out to be capable of detecting pathogen-induced biophysical specific changes in the plant leaf and canopy [27]. Since then, however, remote sensing technologies have significantly progressed. Modern hyperspectral imaging sensors with super spatial, spectral, and radiometric resolutions, offer enhanced capabilities to detect and map disease symptoms on a large scale. These sensors capture reflectance characteristics of the target materials and the reflected light recorded with a high spectral and spatial resolution [28]. The recent advances in hyperspectral imaging sensors are expected to improve disease detection because it allow a pixel-wise attribution of disease-specific symptoms and healthy tissue [29]. In this context, different spectral used to evaluate the vegetation status both quantitatively and qualitatively and spectral vegetation indices (SVIs) are among the most common [28].

A recent study from 2020 demonstrates the possibilities of automatic classification of cotton root rot disease based on Unmanned Aerial Vehicles (UAV) [30]. In R.Naidu (2009), the authors used leaf reflectance differences in the visible (VIS) and near-infrared (NIR) spectrum to predict in advance grapevine infection by *leafroll-associated virus-3*, even though foliar symptoms were not visible yet [31]. Albetis et al., 2017, reported an innovative method to detect *Flavescence dorèe in grapevines* using multispectral images acquired from UAV [32]. Several studies have confirmed the potential of spectral data in early plant pathology detection in different crops [27, 32–37]. Similarly, several studies demonstrated the possibility to distinguish diseased plants from healthy in a reliable way through hyperspectral data in multiple crops [34, 38–40], from which our research took inspiration.

In this study, we have analysed the leaf level reflectance of grapevines *cv.* Teroldego Rotaliano from diseased, healthy, and asymptomatic plants to understand whether there are characteristic spectral changes, across the visible and NIR domains, associated with the infection. We assumed that leaf reflectance provide relevant information to identify *Armillaria* infections in grapevines even though foliar symptoms are not visible yet.

1. Materials and Methods

1.1 Study site

The study was carried out in the Piana Rotaliana (**Error! Reference source not found.**), located in northeast Italy. The Piana Rotaliana is a winegrowing region where *Armillaria* mellea has been a grave problem for several years [18]. The surface is predominantly cultivated with the native red grape variety named Teroldego Rotaliano (about 2000 ha). The soil is characterized by a good water drainage capacity [23], and it

Preprints (www.preprints.org) | NOT PEER-REVIEWED | Posted: 11 May 2021 doi:10.20944/preprints202105.0246.v1

is classified as Post-glacial Alpine [41]; formed in the Pleistocene age by deposits coming from glaciers, landslides, rock glaciers, alluvial debris, with a sandy and gravelly texture.

The selected vineyard is located on the northeast of Piana Rotaliana (46°13'36''N, 11°04'39''E) at 250 m a.s.l. and it was planted in 2005 with the native grape variety Teroldego Rotaliano. The vines were grafted into Teleki 5C rootstock, while the training system was the double pergola. The vine spacing was 5 m x 0.8 m, the rows-oriented ca. east-west. We found the typical fan mycelium attributable to *Armillaria* spp. in several plants within the vineyard and more rarely rhizomorphs in their collars. The vineyard was uprooted at the end of the season 2019, and this allowed us to collect and thoroughly examine the vine roots.

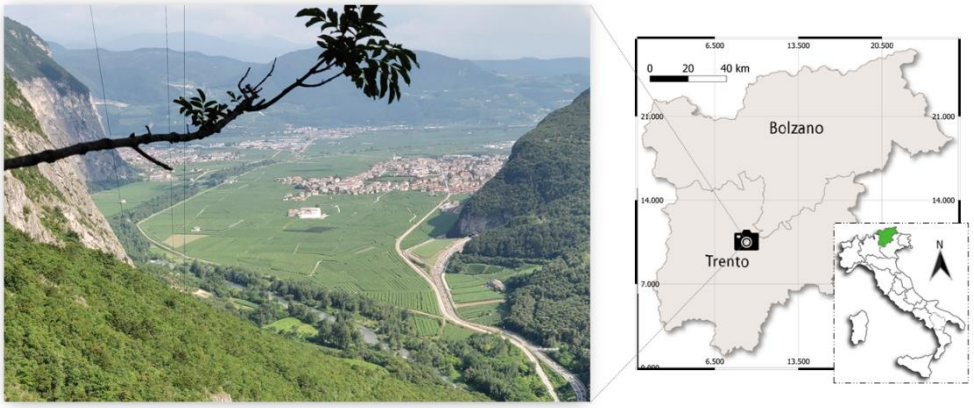

Figure 2. Photo of the winegrowing region Piana Rotaliana located in Trentino region in the northeast side of Italy. From the author, Tor di Visione, (TN), 26-07-2019.

1.2 Foliar sampling

We collected three fresh leaves for each plant on the first week of September 2019, (between 9 p.m. and 11 p.m.). Once detached, the leaves were immediately placed in a refrigerated thermic box at 6°C, then transported to the Spectra lab and stored in darkness at 6°C, before spectral measurements were taken [42]. They were analysed within two hours after field collection. We collected the leaves from the first branch of lateral shoots, generally located between the third and the fourth vineyard trellis wires. We harvested exclusively mature leaves and with a well-exposed upper sheet to sunlight. Moreover, we made sure they were physically intact, apparently healthy on both faces, and they all had approximately homogeneous sizes. Furthermore, plants suspected to be infected by other pathogens were previously excluded.

1.3 Root sampling and inspection

The grapevines were uprooted on the first week of October 2019 using a mechanical excavator. Plant roots were visually assessed, and three portions about 7-8 cm long with a diameter from 1.5 to 3.0 cm taken as a sample for each plant. The portions were chosen from rot or suspected areas. Roots without any evidence of root rot were also collected. We thoroughly washed the samples using fresh and clean water to remove soil debris and disinfected them with the following procedure. They were soaked into a backer with a solution of 30% of a commercial preparation of sodium hypochlorite (NaOCl concentration 5%), 70% of sterile water and 0.01% of Tween-20 for 5 minutes, while the liquid was kept with agitation by a magnetic anchor at room temperature. After disinfection, the roots were washed twice for two minutes with sterile water into a sterile backer and then rinsed. At this point, they were incubated into humid chambers made of transparent sterile nylon bags inflated by air and wet paper inside. We kept humid chambers in closed boxes placed into a dark room for about a month until the final visual disease assessment based on mycelium growth. For the species identification, we relied on Pertot et al. 2008, [43].

Preprints (www.preprints.org) | NOT PEER-REVIEWED | Posted: 11 May 2021 doi:10.20944/preprints202105.0246.v1

1.4 Plant classification

For the plant grouping, we matched the foliar and root symptoms of each vine, as in Figure 3. Healthy plants without symptoms either in canopy and roots, diseased plants with symptoms in leaves and the presence of *Armillaria mellea* in roots, asymptomatic plants without any foliar symptoms but infected by the pathogen and in closest proximity of the diseased ones. In total, we selected 35 grapevines as sample, from which 7 were healthy, 12 diseased, and 16 asymptomatic.

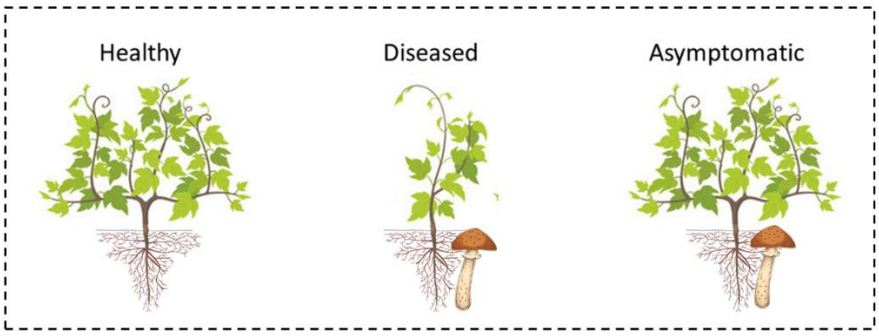

Figure 3. Plant classification illustration; "Healthy" with no symptoms in leaves and roots; "Diseased" symptomatic in both roots and leaves; "Asymptomatic" with symptoms in roots but not in leaves.

1.5 Hyperspectral data acquisition

We used Hyperspectral camera Specimen IQ (Specim, Spectral Imaging Ltd., Oulu, Finland) to measure leaf reflectance. The imaging sensor has a wide variety of applications in remote sensing and precision agriculture. Specim IQ is used to study, in a non-invasively manner, the physiology, architecture, and biochemistry of crop plants or natural vegetation in different environmental conditions and on different scales. For instance, it was implemented for stress detection in plant phenotyping processes and in plant pigment composition studies. Specim IQ acquires the reflected electromagnetic radiation from an object in 204 narrow bands with a spectral range from 397 nm to 1003 nm and a spectral resolution of 7 nm, spectral sampling of 3.5 nm. It performs the measurements by lines scanning 512 pixels and record the image in square with a resolution of 512 x 512 px. The sensor is portable and easy to use, and it can be considered a novel valuable tool for hyperspectral imaging use in the context of plant research and phenotyping strategies [28]. In a recent publication, the sensor was used to detect a common root rot pathogen (*Bipolaris sorokiniana*) affecting the seedlings of wheat [44]. Analogously, Barreto et al., 2020, used this sensor for measuring the root rot disease incidence in celery leaves caused by *Rhizoctonia solani* [45].

In our experiment, Specim IQ was placed on its tripod ground base at 74 cm from the ground and nadir images were collected. The measurements were conducted in a dark room, where light was provided by the two Helder Systemlicht C12 halogen lamps (Helder Systemlicht GmbH, Runkel/Lahn, Germany) placed towards the leaves at an eight of 120 from the ground level. The camera shutter speed was set at 13 milliseconds per pixel, corresponding to 36 seconds per photo. We performed spectral data acquisition including three leaves in each image. The leaves were placed on the ground with the upper surface oriented upwards, as shown in **Error! Reference source not found.**, and arranged with the Spectralon panel nearby used for white calibration. We cut petioles to properly expand the leaves on the ground before spectral analyses.

We analysed the images using the ENVI software (L3Harris Geospatial Solutions Inc., Broomfield CO, USA). First, we extracted the leaves as region of interest (ROI) and excluded background pixels. Then, we calculated the mean reflectance of the leaves, by averaging all pixel values included in the ROI. Noisy bands at the tails, from 397 nm to 423 nm and bans from 954 nm and 1003 nm were eliminated minimizing the background noise [45].

Preprints (www.preprints.org) | NOT PEER-REVIEWED | Posted: 11 May 2021 doi:10.20944/preprints202105.0246.v1

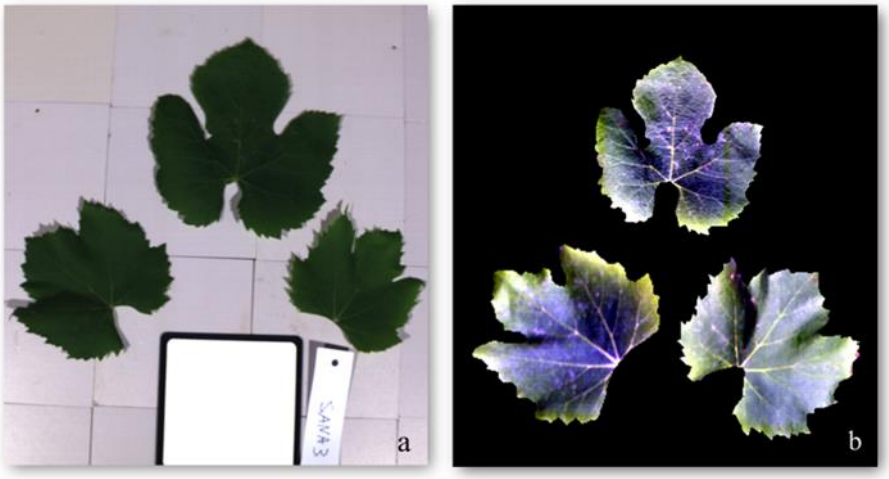

Figure 4. Panel (a) shows a sample of RGB photo of three leaves made with the Specim IQ camera. Panel (b) shows a sample of the hyperspectral image made with Specim IQ of the same leaves.

We calculated a set of 18 vegetation indices (VIs). In this study, we selected VIs potentially capable of discriminating against infected and uninfected vines. Table 1 includes the equations and the references for every selected VIs. Some VIs is used in the literature to detect leaf chlorophyll content (NDchl, REIP3, LCI, Chlred-edge, Vog2, SR750/710), while others are correlated with anthocyanins content (mARI, ARI), and carotenoids content (mCRIRE). Further computed VIs are normally used to retrieve other key vegetation parameters e.g., plant status or biomass (NDVI, GNDVI, AVI, MGVI, DVI, GDVI, OSAVI). Lastly, the index Ctr4 linked to plant-related stresses [46], and the index WBI linked to the water content [47] were computed.

Table 1. Vegetation indices used for measuring reflectance changes between leaves from asymptomatic, diseased, and healthy of *armillaria*-diseased grapevines.

Number	Vegetation Index	Abbreviation	Equation	Related to	Reference
1	*Anthocyanin reflectance index*	ARI	$(R_{551})^{-1} - (R_{705})^{-1}$	*anthocyanins*	[48]
2	*Modified anthocyanin reflectance index*	mARI	$((R_{551})^{-1} - (R_{710})^{-1}) \times R_{951}$	*anthocyanins*	[49]
3	*Carotenoid Reflectance Index red-edge*	mCRIRE	$((R_{520})^{-1} - (R_{700})^{-1}) \times R_{951}$	*carotenoid*	[49]
4	*Normalized Difference Chlorophyll*	NDchl	$(R_{925} - R_{710})/(R_{925} + R_{710})$	chlorophyll	[50]
5	*Red-Edge Inflection Point 3*	REIP3	$\left(((R_{665} + R_{783})/2) - R_{705}\right)/(R_{740} + R_{705})$	*chlorophyll*	[51]
6	*Leaf Chlorophyll Index*	LCI	$(R_{850} - R_{710})/(R_{850} + R_{680})$	*chlorophyll*	[52]

Preprints (www.preprints.org) | NOT PEER-REVIEWED | Posted: 11 May 2021 doi:10.20944/preprints202105.0246.v1

7	*Vogelmann indices 2*	Vog2	$(R_{734} - R_{747})/(R_{715} + R_{726})$	*chlorophyll*	[27]
8	*Zarco-Tejada & Miller*	SR750/710	R_{750}/R_{710}	*chlorophyll*	[53]
9	*Chlorophyll Red-Edge*	Chlred-edge	$(R_{771}/R_{711})^{-1}$	*chlorophyll*	[49]
10	*Difference Vegetation Index*	DVI	R_{951}/R_{640}	*vegetation*	[54]
11	*Normalized Difference Vegetation Index*	NDVI	$(R_{932} - R_{604})/(R_{604} + R_{932})$	*vegetation*	[54]
12	*Misra Green Vegetation Index*	MGVI	$-0.386(R_{500}) - 0.530(R_{600}) + 0.535(R_{800}) + 0.532(R_{951})$	*vegetation*	[54]
13	*Green Normalized Difference Vegetation Index*	GNDVI	$(R_{570} - R_{800})/(R_{570} + R_{800})$	*vegetation*	[55]
14	*Ashburn Vegetation Index*	AVI	$2.0 \times (R_{951}) - (R_{600})$	*vegetation*	[54]
15	*Green Difference Vegetation Index*	GDVI	$R_{566} - R_{902}$	*vegetation*	[56]
16	*Optimized Soil Adjusted Vegetation Index*	*OSAVI*	$(1 + 0.16)/((R_{902} - R_{672})/(R_{902} + R_{672} + 0.16))$	*vegetation*	[53]
17	*Simple Ratio Carter4*	Ctr4	R_{710}/R_{760}	*stress*	[57]
18	*Water Band Index*	WBI	R_{970}/R_{902}	*water content*	[47]

1.6 Statistical analyses

In a preliminary analysis, we calculated the standard deviation within each group of plants with the following formula:

$$\sigma = \sqrt{\frac{\sum(X - \overline{X})^2}{n}}$$

Where X represent the single plant reflectance, x the group-averaged reflectance, and n the number of plants within the group.

Afterwards, we performed an inferential statistical analysis in three different steps, Figure 5**Error! Reference source not found.**. In step 1, we determined the most relevant wavelengths to discriminate diseased, healthy, and asymptomatic groups. In step 2, we computed and selected the VIs most relevant to separate the groups of plants. In step 3, we employed a classification analysis using the most discriminant variable among both wavelengths and VIs. For the wavelengths we used the same statistical approach used in Manevski et al., 2017, to discriminate different types of vegetation [58]. In this approach, we performed both parametric and non-parametric ANOVA (Kruskal Wallis) tests for every single wavelength with their respective cross-validation tests Tukey HSD and

Preprints (www.preprints.org) | NOT PEER-REVIEWED | Posted: 11 May 2021 doi:10.20944/preprints202105.0246.v1

Wilcox. To select the most sensible vegetation indices we relied on Naidu et al., 2009, and Avola et al., 2019; however, since not all the data were normally distributed we performed a non-parametric ANOVA test in addition to the parametric ANOVA [31, 59]. Data assumptions for the ANOVA test were checked using Shapiro and Bartlett tests. Finally, in order to classify the groups of plants, Linear Discriminant Analysis (LDA) was performed using the combination of the first 5 most discriminant variables among VIs and wavelengths [37, 59]. The p-values of VIs are reported in Table A1 and TableA2, while for the wavelengths the p-values are reported in Table S1. Data assumptions for LDA were checked using Shapiro and boxM tests, and statistical transformation were made where required, the results may be consulted in table S2. We used 65% of the dataset as training and 35% as a validation set. Finally, we calculated the Overall Accuracy using the following formula:

$$Overall\ Accuracy\ (\%) = \left[\frac{(TP + TN)}{(TP + TN + FP + FN)}\right] \times 100$$

where TP and TN are true positive (diseased correctly detected) and true negative (healthy plants correctly detected), respectively. FP and FN mean false positive (healthy plants detected as diseased) and false negative (diseased plants detected as healthy), respectively. All the statistical analyses were carried out using R studio.

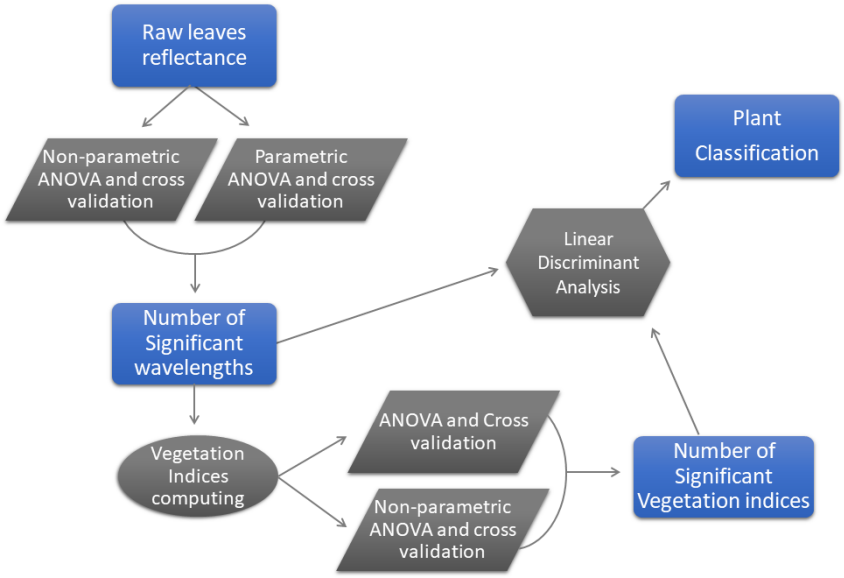

Figure 5. Analytical framework of implemented statistical analyses to select specific sensible narrow bands and VIs and validate the *Armillaria* infected plats classification in grapevines.

2. Results

In both diseased and asymptomatic vines, after the incubation period, we found the typical mycelium of *Armillaria* growing under root bark as well as the external fan mycelium in at least one out of three portions, Figure 6.

Preprints (www.preprints.org) | NOT PEER-REVIEWED | Posted: 11 May 2021 doi:10.20944/preprints202105.0246.v1

Figure 6. Panel (a) shows an example of the typical mycelial fan of *Armillaria* spp. found on incubated roots; Panel (b) shows an example of the *Armillaria* subcortical mycelium; Panel (c) shows the longitudinal bark breaking caused by the mycelium expansion. From the author, Edmund Mach Foundation.

Figure 7 shows the averaged leaf reflectance of healthy, diseased, and asymptomatic plants. There are noticeable differences between the groups across the NIR spectral region ranging from 750 to 951 nm, Figure 7c. Slighter differences are also observed in Figure 7a in the green spectrum (from 530 to 630 nm) and in Figure 7b red edge (from 700 to 725 nm). The ribbons behind each group represent their standard deviations.

Figure 8a highlights the spectral differences between asymptomatic and healthy and diseased plants. The differences between healthy and diseased groups increases together with the wavebands along the NIR region reaching the maximum difference at 951 nm. Slightly smaller peaks of reflectance appear in asymptomatic plants observed near 566nm and 705nm. In Figure 8b, shows the standard deviation within each group of plants and therefore the dispersion of data.

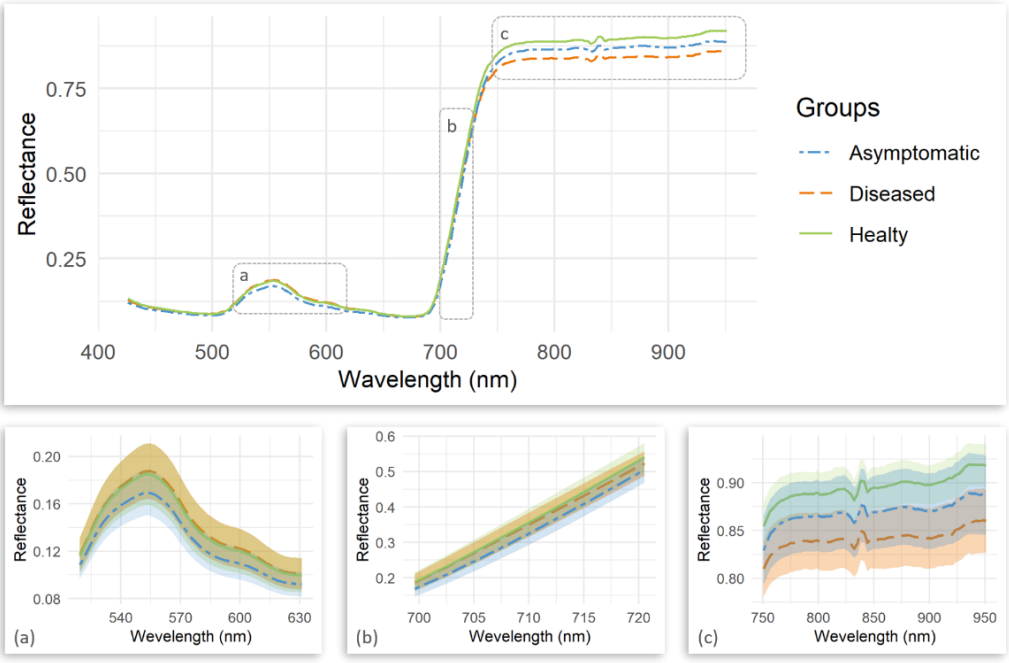

Figure 7. Mean hyperspectral signatures of the three plant groups plus their standard deviations in the ribbons. Panel (a) highlights the signatures in the green spectrum, panel (b) in red-edge, and panel (c) in the NIR spectrum.

Preprints (www.preprints.org) | NOT PEER-REVIEWED | Posted: 11 May 2021 doi:10.20944/preprints202105.0246.v1

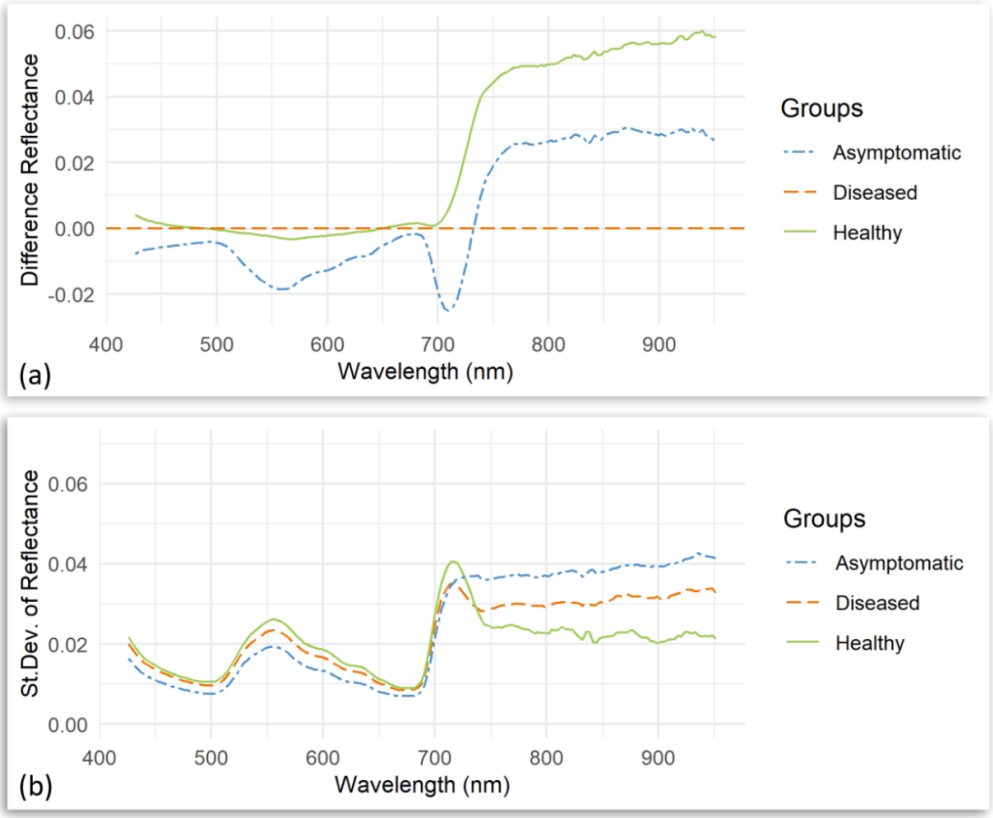

Figure 8. Panel (a) shows mean reflectance of healthy minus diseased plants, and asymptomatic minus Diseased plants; Panel (b) shows the standard deviations, within each group of plants.

In Figure 9 we reported the matrix of bands, with their level of significance to discriminate between the groups of plants. Wavelengths in green are characterised by a high discrimination power, whereas grey wavelengths by a low discrimination power according to ANOVA tests.

The parametric ANOVA test resulted more sensitive than the non-parametric test, detecting a higher number of significant and highly significant wavelengths in all the three two-by-two comparisons, which is consistent with the results of [58]. Nevertheless, both tests confirmed the differences to be significant between several narrow bands. In particular, diseased versus healthy plants showed highly significant differences in the NIR spectrum (from 750nm to 951nm), with the lowest p-values in 889nm, 920nm, and 902nm. Similarly, significant differences in the NIR region were found between asymptomatic and diseased plants according to the parametric ANOVA test results. Asymptomatic plants resulted significantly different in the red-edge spectrum from the other two groups with the lowest p-value at 705nm. Moreover, asymptomatic plants compared to diseased showed significant differences in the green spectrum with the lowest p-value at 566nm.

Preprints (www.preprints.org) | NOT PEER-REVIEWED | Posted: 11 May 2021 doi:10.20944/preprints202105.0246.v1

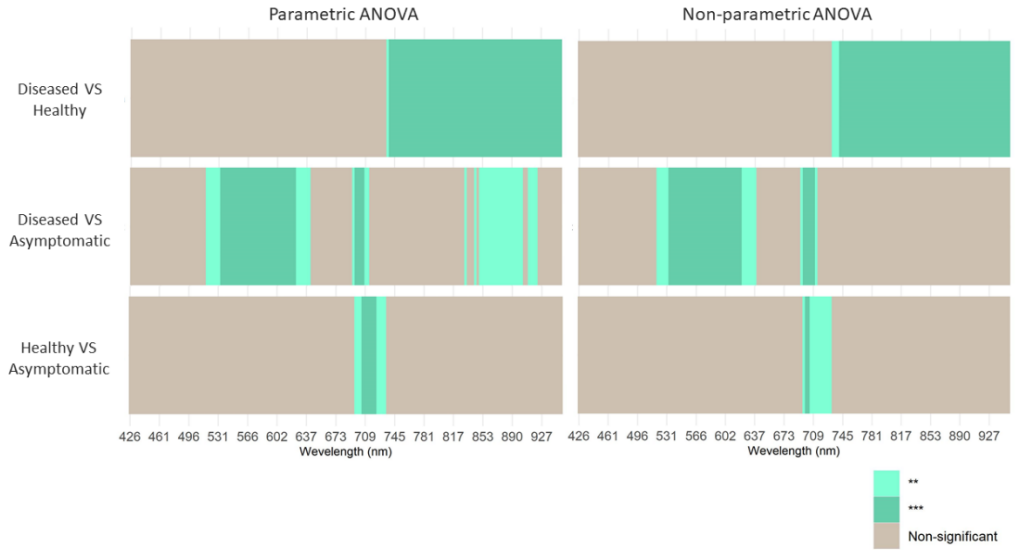

Figure 9. Sensitivity matrix of vegetation spectral discrimination based on the type of statistical test. Parametric versus nonparametric analysis of variance (ANOVA) for the three spectral libraries. P-value < 0.025 (**), P-value < 0.01 (***).

Results of non-parametric and parametric statistical analyses concerning the VIs are reported respectively in TableA 1, and TableA 2. Although, all VIs, except for WBI, produced highly significant results in the ANOVA test (P-value < 0.01), any of the VIs was capable to separate the whole three groups singularly; suggesting that a plant classification may be possible only with a combination of the indices. Diseased and healthy plants exhibited differences in the vegetation vigour related indices, such as GNDVI, GDVI, MGVI, OSAVI, NDVI, AVI, DVI but also in mCRIRE and mARI. Healthy and asymptomatic plants showed the highest differences in the indices: Ctr4, REIP3, Chlred-edge, SR750.710, Vog2. While all the VIs, except for the mCRIRE and WBI, showed significant differences between diseased and asymptomatic plants. Figure 10 illustrates the VIs with cross-validation results between the plant groups.

Preprints (www.preprints.org) | NOT PEER-REVIEWED | Posted: 11 May 2021 doi:10.20944/preprints202105.0246.v1

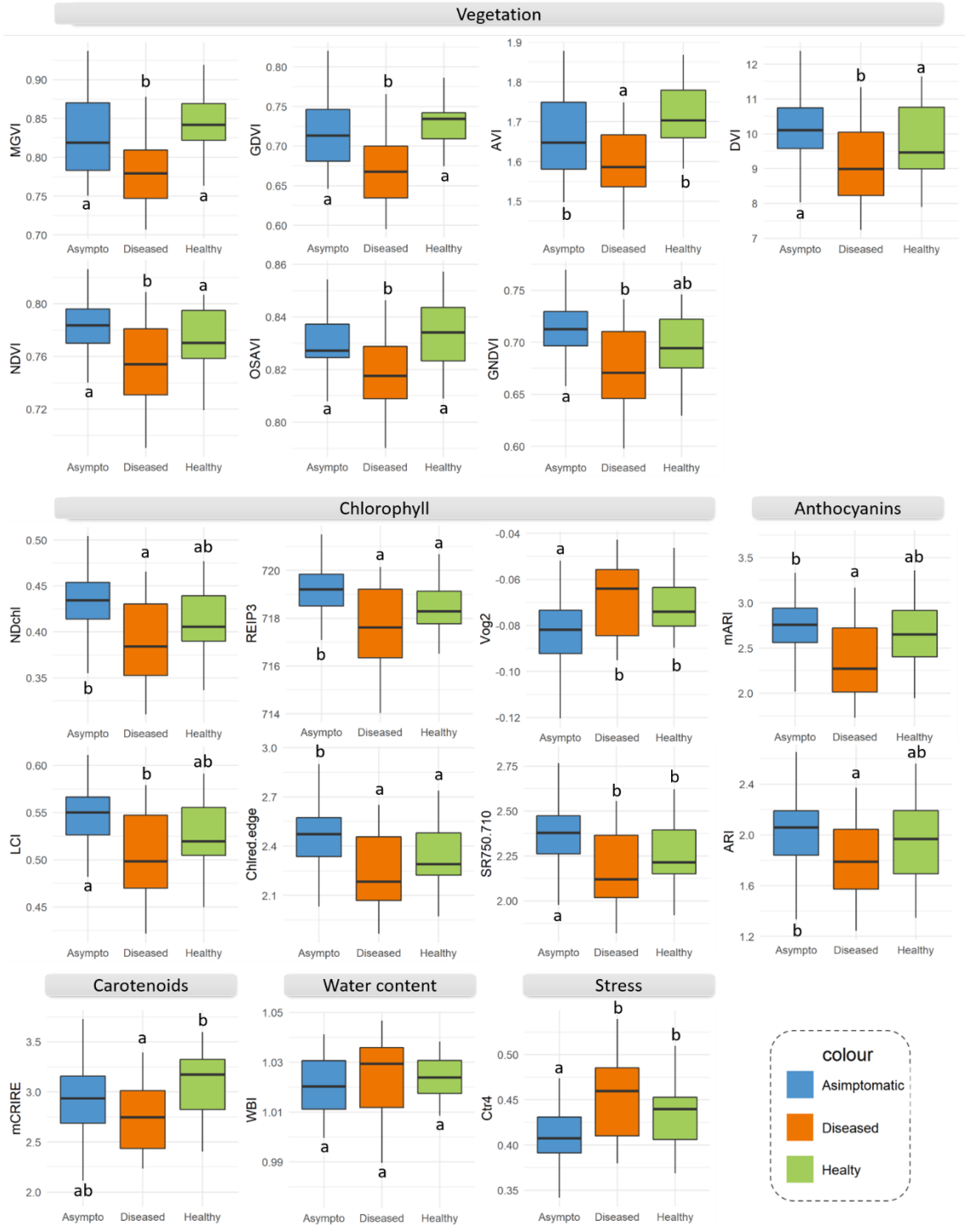

Figure 10. Most significant vegetation indices with their quantiles, mean and maximum values for each group of plants. Within the single vegetation index, the plant groups are identified with letters showing significant differences at the Tukey (HSD) test (p-value < 0.05).

The results of LDA classification are illustrated in Table 2. It appears that the use of the selected wavelengths and VIs produces good classifications, supporting the theory that hyperspectral data is capable to identify *Armillaria mellea* infection.

Table 2. Classification accuracies based on LDA using combinations of variables.

Groups	**Variables used**	**Overall accuracy**
Healthy - Diseased	*GDVI, MGVI, AVI, OSAVI, R920*	*85%*

 doi:10.20944/preprints202105.0246.v1

Healthy - Asymptomatic	*R705, R711, R708, R714, R717*	*84%*
Healthy - Asymptomatic - Diseased	*GDVI, NDchl, MGVI, OSAVI, GNDVI*	*70%*

4. Discussion

The NIR reflectance has an increasing pattern in all three groups starting from diseased, asymptomatic, up to healthy plants. In particular, the high reflectance values along the NIR spectrum from 750 nm up to 951nm characterized healthy from diseased leaves, with the most relevant peaks in 902nm, 920nm and 889nm. This conclusion is coherent with the literature as it is well known that the NIR light is not absorbed by leaf pigments but rather reflected in healthy leaves [42, 60–63]. It appears that the values in the NIR are much more valuable than the VIS spectral range to discriminate diseased from healthy plants. Similar conclusions were also drawn in Zhang, et al., 2005, for the detection of tomatoes stress induced by the fungal pathogen *Phytophthora infestans* [64]. The NIR shoulder is related to internal leaf structures and its reflective scattering is principally due to the air in leaf cell walls and to the differences in leaf cellular constituents [65–67]. Reflectance in the NIR-shoulder domain also can be used for assessing leaf structure, leaf deterioration and senescence [66]. Consequently, the reduced NIR reflectance observed in the canopy of root rot affected plants may be attributed to leaf structural changes induced by wilting processes [68]. Moreover, the NIR response is also related to the leaf water content [69], despite, in our results, we did not observe relevant differences in WBI index between the plant groups.

Overall, according to the considered VIs, we can assume that diseased plants are characterized by lower vegetation vigour and leaf pigment content. Consistently, Nogales et al., 2009, using a chlorophyll meter SPAD 502, assessed that grapevines artificially inoculated with *Armillaria mellea,* that showed evident foliar symptoms, have a significantly lower foliar chlorophyll content than healthy plants [70], which presuppose divergences in the leaf reflectance features. As suggested by the mCRIRE index, diseased plants may also have a lower content of carotenoids than healthy plants. These pigments contributes to the light-harvesting in the green spectrum as well as the photosynthetic systems protection [49].

Diseased plants exhibited lower values than healthy plants in GDVI, MGVI, NDVI, AVI, DVI and OSAVI indices. Since these VIs are strongly correlated to the vegetation biomass [53–56] and considering the reduced biomass production of diseased plants [18], we can hypnotize a variation in the leaf biomass, leaf dry weight, and specific leaf area (SLA) in healthy *vs*. diseased plants. Among these indices, the OSAVI was used in Reynolds et al., 2012, and Barreto et al., 2020, to discriminate healthy *vs*. infected plants of another rot root disease caused by *Rhizoctonia solani* fungi in sugar beet [45, 68]. In this pathosystem, OSAVI resulted negatively correlated with the severity of *Rhizoctonia* crown root rot, suggesting the possibility of remotely detect diseased plants when at least 26 to 50% of the root surface are rotted. Similarly, in our results, OSAVI was one of the most significant VIs to separate healthy and *Armillaria*-diseased vines (p-value = 0.00017), remarking the relevant role of the OSAVI index in root rot disease detection.

For NDVI, Pérez-Bueno et al., 2019, reported lower values in avocado trees affected by the white root rot caused by the *Rosellinia necatrix* fungi using a multispectral sensor on UAV [71], consistently, we found lower NDVI in grapevine affected by *Armillaria* root rot. Granum et al., 2015, suggested that, in this pathosystem, the leaf metabolism of avocado trees is significantly affected in response to the loss of radical system functionality of diseased plants [72]; supporting that a radical pathogen can induce, throughout systemic effects inside the host, changes in leaf metabolism and leaf light response even though the pathogen is not a direct pathogen of leaves [73]. As a matter of fact, Candiago et al., 2015, while studying the possible applications of multispectral images from UAV for precision farming, found out that the area of the vineyard they had analyzed reporting the lowest values of GNDVI, NDVI, and SAVI was mostly infected by *Armillaria mellea* root rot and trunk disease [82]. Perhaps not unexpectedly, the VIs

 doi:10.20944/preprints202105.0246.v1

reported in Candiago et al., 2015, were just the same ones that we observed to be sensible in our experiments.

On the other hand, despite the *Armillaria* roots colonization, we can assume that the photosynthetic capacity of asymptomatic plants was not as affected as for the diseased ones, probably because of the earlier disease stage in asymptomatic plants. In fact, the asymptomatic group stood out from diseased due to its lower reflectance in the green (near 566nm), red edge (near 705nm), as well as a slightly higher reflectance in the infrared (near 902nm) according to parametric ANOVA. Again, asymptomatic *vs*. diseased groups exhibited a higher plant vigour (GDVI, MGVI, OSAVI, NDVI, AVI, GNDVI, DVI), chlorophyll content (REIP3, Chlred-edge, NDchl, DPI, LCI, SR750/710, as well as anthocyanins content (mARI, ARI).

However, the encouraging result towards an early diseased detection was that asymptomatic plants, apparently indistinguishable from healthy ones using a visual assessment, showed significant differences in the red-edge spectrum from 705 nm to 720nm. Consequently, those VIs computed from narrow bands within the red-edge interval (REIP3, Chlred-edge, SR750.710) resulted significant in asymptomatic *vs*. healthy plant discrimination as well. This observation represents an essential signal for the early disease detection, allowing us to classify leaves of asymptomatic from healthy plants. The red-edge domain is correlated with chlorophyll and nitrogen leaf content [74–76]. Nevertheless, we do not exclude that the spectral variations are triggered by a concentration of metabolites in leaves that are directly involved in plant defence strategies [70, 77].

Recent studies reported that leaf biochemical changes occur after the *Armillaria* infection, which in turn may be involved in the leaf optical properties modifications. Camprubi et al., 2020, investigated the metabolomic profile of loquat plants in response to *Armillaria* mellea inoculation following mycorrhizal fungi colonization [77]. They found metabolites directly involved in plant defence, such as DIMBOA and conjugated isoflavone phytoalexins in infected plants as well as a complex modulation of metabolites such as: fucose, ADP-glucose, UDP-glucose, and down-accumulation of lipids and fatty acids in *Armillaria*-infected plants. In Nogales et. Al., 2009, was observed a decrease in polyamines (PA) concentration in leaves of *A. mellea*-infected grapevines, with a subsequent increase in mycorrhized plants [70]. Low PA levels are a characteristic of senescent tissues with low cellular division activity [78]. Perhaps not unexpectedly Heritage et al., 2010, advocates that PA induce leaf reflectance changes either in the VIS and NIR regions [79]. While Minocha et al., 1997, already demonstrated that changes in polyamine levels in response to stress could be used as an early warning tool for assessing and predicting tree health before the visual symptoms appear [80].

It is well known from the literature that biochemical changes in leaves induce variations in leaf spectral properties, including the red edge domain [73, 81]. However, a metabolite characterization is essential to understand how specific metabolites affect the leaf hyperspectral signature. A broad job was done by Vergara-Diaz et al., 2020 to asses which wavebands of the spectrum are related to the specific metabolites or groups of metabolites content in wheat leaves [81]. The authors found out that red-edge (around 680–780 nm) is one of the most relevant domain to retrieve the metabolites content in leaves together with the NIR and SWIR regions, in particular for nitrogen and protein content [81]. This observation indicate that a leaf metabolites alteration involved in the red-edge reflectance variation of asymptomatic plants affected by *Armillaria mellea* may be not excluded.

Finally, the linear discriminant analysis produced a reliable level of accuracy of 85% in classifying healthy and *Armillaria*-diseased plants. As we expected, the accuracy decreased to 70% when we introduced a third classification group made by asymptomatic vines. However, it is a great encouragement that 84% of reliable accuracy was also obtained in the healthy *vs.* asymptomatic plants, as this comparison is more linked to an applicative approach of this technique.

Preprints (www.preprints.org) | NOT PEER-REVIEWED | Posted: 11 May 2021 doi:10.20944/preprints202105.0246.v1

5. Conclusion

In this study, we have shown that spectral reflectance techniques in support of visual assessment can be a promising tool for *Armillaria* root rot disease detection from which modern viticulture may benefit. Therefore, spectral sensors may be used to increase the accuracy of non-specific *Armillaria* symptoms interpretation in the field. In addition, since asymptomatic plants represent the early stage of the disease, the detection of them through hyperspectral data in areas neighbouring to diseased plants would allow the implementation of a Decision Support System in a modern Precision Agriculture System for the earliest action to contain the disease. For instance, the possibility to remove earlier affected plants and their roots, with a consequent reduction of *Armillaria* inoculum in the soil, and the limitation of chemical interventions in the vineyard before replanting.

Spectral sesnors would allow cost-effective and non-destructive measurements in the field. On the one hand, this technique could be implemented on simple and cheap sensors similar to SPAD for quicker in situ spectral observations using wavelengths in the green (566 nm), red edge (705 nm), and NIR regions (902 nm). On the other hand, multispectral sensors installed on UAV could be used to map the *Armillaria* infection, providing precious information on the disease distribution and its spreading.

To our knowledge, this study represents the first report on the possibility of using hyperspectral data for root rot disease diagnosis on woody plants. Despite the encouraging results obtained in plant classification, it is necessary to carry out further studies on different grape varieties both red and white in order to validate the spectral differences of *Armillaria*-infected vines and develop a general prediction model. Thus, a further research is expected to assess the effect of *Armillaria* artificial infections on grapevine seedlings grown in greenhouse under controlled environmental conditions and in different grape varieties.

Supplementary Materials: Table S1: Parametric ANOVA, non-parametric ANOVA, and their relative cross validation tests results for single wavelength. Table S2: Data assumptions results for Linear discriminant analysis. Video S1: High distribution of early red canopy in grapevines due to *Armillaria* root rot in Piana Rotaliana (11 October 2019). Early red canopy symptoms often appear in post-harvesting in red grape variety that already has been highly compromised by the pathogen.

Author Contributions: For research articles with several authors, a short paragraph specifying their individual contributions must be provided. Conceptualization, FC, NLP; methodology, FC., NLP; software, FC, HAI, LV; validation, FC, NLP; formal analysis, FC; investigation, FC, NLP; resources, HAI, MLM; data curation, FC; writing—original draft preparation, FC; review, NLP, HAI, LV, MLM; visualization, FC, NLP; supervision, NLP; project administration, FC, NLP. All authors have read and agreed to the published version of the manuscript.

Funding: This research received no external funding.

Acknowledgments: We gratefully acknowledge the Edmund Mach Foundation for having made their laboratories available. We would also like to thank Roberto Zorer, Farid Melgani, and Daniele Prodorutti, which thanks to their experience, have given us crucial advice and tips. Thanks to the whole laboratory staff, particularly Franca Valentini and Lorena Ress for their essential help. We would also like to acknowledge the director of the "Cantina Rotaliana di Mezzolombardo" Leonardo Pilati, who enthusiastically grasped the idea of this study. Thanks to Saverio D.V. that supported us with his great passion, and finally, thanks to Metacortex s.r.l. and Rino Goller for their helpful collaboration.

Conflicts of Interest: The authors declare no conflict of interest.

Appendix A

TableA 1. Non-parametric ANOVA and its relative cross validation results for the VIs. P-value < 0.05 (*), P-value < 0.025 (**), P-value < 0.01 (***).

N°	Index	P-value	Diseased VS	Healthy VS	Healthy VS

Preprints (www.preprints.org) | NOT PEER-REVIEWED | Posted: 11 May 2021 doi:10.20944/preprints202105.0246.v1

			Asymptomatic	Asymptomatic	Diseased
			Cross validation P-adj		
1	GDVI	0.000004 (***)	0.00005 (***)	0.52294	0.00002 (***)
2	MGVI	0.00004 (***)	0.00130 (***)	0.27417	0.00009 (***)
3	OSAVI	0.00009 (***)	0.00016 (***)	1	0.00259 (***)
4	NDchl	0.00011 (***)	0.00009 (***)	0.05128	0.35577
5	mARI	0.00012 (***)	0.00004 (***)	0.87102	0.05249
6	Ctr4	0.00016 (***)	0.00019 (***)	0.02559 (*)	0.60489
7	Chlred-edge	0.00016 (***)	0.00018 (***)	0.03003 (*)	0.58745
8	REIP3	0.00019 (***)	0.00045 (***)	0.00916 (***)	0.95927
9	SR750/710	0.00020 (***)	0.00026 (***)	0.02886 (*)	0.58745
10	GNDVI	0.00021 (***)	0.00014 (***)	0.19992	0.15410
11	NDVI	0.0002116 (***)	0.00008 (***)	0.49839	0.1367105
12	LCI	0.00023 (***)	0.00023 (***)	0.05320	0.43261
13	AVI	0.00025 (***)	0.03044 (*)	0.09668	0.00014 (***)
14	DVI	0.00039 (***)	0.00014 (***)	0.88900	0.11608
15	Vog2	0.00122 (***)	0.00155 (***)	0.04942 (*)	1.00000
16	mCRIRE	0.00219 (***)	0.05001	0.25925	0.00276 (***)
17	ARI	0.00908 (***)	0.00451 (***)	0.98258	0.62269
18	WBI	0.155332	0.2268854	0.7044217	1

TableA 2. Parametric ANOVA and its relative cross validation results for the VIs. P-value < 0.05 (*), P-value < 0.025 (**), P-value < 0.01 (***).

N°	Index	P-value	F-value	Diseased VS Asymptomatic	Healthy VS Asymptomatic	Healthy VS Diseased
				Cross validation P-adj		
1	GDVI	6.6E-07 (***)	16.42	1.4E-05 (***)	5.0E-01	8.7E-06 (***)
2	NDchl	1.2E-05 (***)	12.69	6.7E-06 (***)	6.3E-02	1.6E-01
3	MGVI	1.3E-05 (***)	12.63	4.3E-04 (***)	3.0E-01	3.9E-05 (***)
4	OSAVI	**1.4E-05 (***)**	**1.3E+01**	**9.6E-05 (***)**	**7.4E-01**	**1.7E-04 (***)**
5	GNDVI	1.5E-05 (***)	12.42	7.6E-06 (***)	1.7E-01	6.6E-02
6	NDVI	**1.7E-05 (***)**	**12.24**	**9.00E-06 (***)**	**2.50E-01**	**4.26E-02 (*)**
7	LCI	1.8E-05 (***)	12.17	1.0E-05 (***)	7.2E-02	1.7E-01
8	Ctr4	2.0E-05 (***)	12.07	1.3E-05 (***)	3.8E-02 (*)	2.8E-01
9	REIP3	2.2E-05 (***)	11.94	1.5E-05 (***)	3.5E-02 (*)	3.1E-01
10	Chlred.edge	2.6E-05 (***)	11.71	2.0E-05 (***)	3.1E-02 (*)	3.6E-01
11	mARI	2.8E-05 (***)	11.62	1.7E-05 (***)	4.3E-01	2.4E-02 (**)
12	SR750.710	3.7E-05 (***)	11.30	2.8E-05 (***)	3.2E-02 (*)	4.0E-01
13	AVI	7.3E-05 (***)	10.47	7.6E-03 (***)	1.0E-01	7.2E-05 (***)
14	DVI	9.1E-05 (***)	10.21	5.4E-05 (***)	4.4E-01	4.3E-02 (*)
15	Vog2	2.7E-04 (***)	8.90	2.6E-04 (***)	3.9E-02 (*)	6.3E-01
16	mCRIRE	2.5E-03 (***)	6.35	6.5E-02	1.9E-01	2.1E-03 (***)
17	ARI	5.5E-03 (***)	5.47	3.7E-03 (***)	4.7E-01	2.8E-01

18	WBI	0.2805945	1.286811	0.3054819	0.5073119	0.9914079

References

[1] Watling, R.; Kile, G. A.; Burdsall jr, H. H. Nomenclature, Taxonomy and Identification. In *Armillaria root desease*; Routledge, 1991; pp 1–9.

[2] Coetzee, M. P. A.; Wingfield, B. D.; Wingfield, M. J. Armillaria Root-Rot Pathogens: Species Boundaries and Global Distribution. *Pathogens*, **2018**, *7* (4), 1–18. https://doi.org/10.3390/pathogens7040083.

[3] Yafetto, L.; Davis, D. J.; Money, N. P. Biomechanics of Invasive Growth by Armillaria Rhizomorphs. *Fungal Genet. Biol.*, **2009**, *46* (9), 688–694. https://doi.org/10.1016/j.fgb.2009.04.005.

[4] Yafetto, L. The Structure of Mycelial Cords and Rhizomorphs of Fungi: A Mini-Review. *Mycosphere*, **2018**, *9* (5), 984–998. https://doi.org/10.5943/mycosphere/9/5/3.

[5] Smith, M. L.; Bruhn, J. N.; Anderson, J. B. The Fungus Armillaria Bulbosa Is among the Largest and Oldest Living Organisms. *Nature*, **1992**, *356* (6368), 428–431. https://doi.org/10.1038/356428a0.

[6] Ferguson, B. A.; Dreisbach, T. A.; Parks, C. G.; Filip, G. M.; Schmitt, C. L. Coarse-Scale Population Structure of Pathogenic Armillaria Species in a Mixed-Conifer Forest in the Blue Mountains of Northeast Oregon. *Can. J. For. Res.*, **2003**, *33* (4), 612–623. https://doi.org/10.1139/x03-065.

[7] Heinzelmann, R.; Dutech, C.; Tsykun, T.; Labbé, F.; Soularue, J. P.; Prospero, S. Latest Advances and Future Perspectives in Armillaria Research. *Can. J. Plant Pathol.*, **2019**, *41* (1), 1–23. https://doi.org/10.1080/07060661.2018.1558284.

[8] La Porta, N.; Capretti, P.; Thomsen, I. M.; Kasanen, R.; Hietala, A. M.; Von Weissenberg, K. Forest Pathogens with Higher Damage Potential Due to Climate Change in Europe. *Can. J. Plant Pathol.*, **2008**, *30* (2), 177–195. https://doi.org/10.1080/07060661.2008.10540534.

[9] Cabrera, O. G.; Molano, E. P. L.; José, J.; Álvarez, J. C.; Pereira, G. A. G. *Cacao Diseases*; Bailey, B. A., Meinhardt, L. W., Eds.; Springer International Publishing: Cham, 2016. https://doi.org/10.1007/978-3-319-24789-2.

[10] Baumgartner, K.; Coetzee, M. P. A.; Hoffmeister, D. Secrets of the Subterranean Pathosystem of Armillaria. *Mol. Plant Pathol.*, **2011**, *12* (6), 515–534. https://doi.org/10.1111/j.1364-3703.2010.00693.x.

[11] Cromey, M. G.; Drakulic, J.; Beal, E. J.; Waghorn, I. A. G.; Perry, J. N.; Clover, G. R. G. Susceptibility of Garden Trees and Shrubs to Armillaria Root Rot. *Plant Dis.*, **2020**, *104* (2), 483–492. https://doi.org/10.1094/PDIS-06-19-1147-RE.

[12] Marsh, R. W. Field Observations on the Spread of Armillaria Mellea in Apple Orchards and in a Blackcurrant Plantation. *Trans. Br. Mycol. Soc.*, **1952**, *35* (3), 201–207. https://doi.org/10.1016/s0007-1536(52)80049-x.

[13] Rizzo, D. M.; Whiting, E. C.; Elkins, R. B. Spatial Distribution of Armillaria Mellea in Pear Orchards. *Plant Dis.*, **1998**, *82* (11), 1226–1231. https://doi.org/10.1094/PDIS.1998.82.11.1226.

[14] Beckman, T. G.; Okie, W. R.; Nyczepir, A. P.; Pusey, P. L.; Reilly, C. C. Relative Susceptibility of Peach and Plum Germplasm to Armillaria Root Rot. *HortScience*. 1998, pp 1062–1065. https://doi.org/10.21273/hortsci.33.6.1062.

[15] Miller, S. B.; Gasic, K.; Reighard, G. L.; Henderson, W. G.; Rollins, P. A.; Vassalos, M.; Schnabel, G. Preventative Root-Collar Excavation Reduces Peach Tree Mortality Caused by Armillaria Root Rot on Replant Sites. *Plant Dis.*, **2020**, *104* (5), 1274–1279. https://doi.org/10.1094/PDIS-09-19-1831-RE.

[16] Donati, I.; Cellini, A.; Sangiorgio, D.; Caldera, E.; Sorrenti, G.; Spinelli, F. Pathogens Associated to Kiwifruit Vine Decline in Italy. *Agric.*, **2020**, *10* (4). https://doi.org/10.3390/agriculture10040119.

[17] Baumgartner, K.; Rizzo, D. M. Spread of Armillaria Root Disease in a California Vineyard. *Am. J. Enol. Vitic.*, **2002**, *53* (3), 197–203.

[18] Baumgartner, K. Root Collar Excavation for Postinfection Control of Armillaria Root Disease of Grapevine. *Plant Dis.*, **2004**, *88* (11), 1235–1240. https://doi.org/10.1094/PDIS.2004.88.11.1235.

[19] Prodorutti, D.; De Luca, F.; Michelon, L.; Pertot, I. Susceptibility to Armillaria Mellea Root Rot in Grapevine Rootstocks

Commonly Grafted onto Teroldego Rotaliano. *Phytopathol. Mediterr.*, **2009**, *48* (2), 285–290. https://doi.org/10.14601/Phytopathol_Mediterr-2738.

[20] Aguín, O.; Abuín, M.; Lozano, F.; Ferreiroa, V.; Corral, M.; Mansilla, J. P. Incidencia y Distribución Del Género Armillaria En Viñedos de Las Cinco Denominaciones de Origen de Vino de Galicia (Noroeste de España). *Rev. Iberoam. Micol.*, **2015**, *32* (1), 13–19. https://doi.org/10.1016/j.riam.2013.10.010.

[21] Ricciolini, M.; Rizzo, D. *Avversità Della Vite e Strategie Di Difesa Integrata in Toscana*; 2007.

[22] Nieuwenhuis, B. P. S.; Billiard, S.; Vuilleumier, S.; Petit, E.; Hood, M. E.; Giraud, T. Evolution of Uni- and Bifactorial Sexual Compatibility Systems in Fungi. *Heredity (Edinb).*, **2013**, *111* (6), 445–455. https://doi.org/10.1038/hdy.2013.67.

[23] Prodorutti, D.; De Luca, F.; Pellegrini, A.; Pertot, I. *I Marciumi Radicali Della Vite*; 2007.

[24] Kwaśna, H.; Szynkiewicz-Wronek, A. Culturable Microfungi Inhibitory to Armillaria Rhizomorph Formation from Fagus Sylvatica Stump Roots and Soil. *J. Phytopathol.*, **2018**, *166* (5), 314–323. https://doi.org/10.1111/jph.12689.

[25] Bendel, N.; Kicherer, A.; Backhaus, A.; Köckerling, J.; Maixner, M.; Bleser, E.; Klück, H. C.; Seiffert, U.; Voegele, R. T.; Töpfer, R. Detection of Grapevine Leafroll-Associated Virus 1 and 3 in White and Red Grapevine Cultivars Using Hyperspectral Imaging. *Remote Sens.*, **2020**, *12* (10), 1–26. https://doi.org/10.3390/rs12101693.

[26] Toler, R. W.; Smith, B. D.; Harlan, J. C. Use of Aerial Color Infrared Photography to Evaluate Crop Disease. *Plant Dis.*, **1981**, 24–31.

[27] Behmann, J.; Steinrücken, J.; Plümer, L. Detection of Early Plant Stress Responses in Hyperspectral Images. *ISPRS J. Photogramm. Remote Sens.*, **2014**, *93*, 98–111. https://doi.org/10.1016/j.isprsjprs.2014.03.016.

[28] Behmann, J.; Acebron, K.; Emin, D.; Bennertz, S.; Matsubara, S.; Thomas, S.; Bohnenkamp, D.; Kuska, M. T.; Jussila, J.; Salo, H.; et al. Specim IQ: Evaluation of a New, Miniaturized Handheld Hyperspectral Camera and Its Application for Plant Phenotyping and Disease Detection. *Sensors (Switzerland)*, **2018**, *18* (2). https://doi.org/10.3390/s18020441.

[29] Mahlein, A. K.; Steiner, U.; Hillnhütter, C.; Dehne, H. W.; Oerke, E. C. Hyperspectral Imaging for Small-Scale Analysis of Symptoms Caused by Different Sugar Beet Diseases. *Plant Methods*, **2012**, *8* (1), 1–13. https://doi.org/10.1186/1746-4811-8-3.

[30] Wang, T.; Thomasson, J. A.; Yang, C.; Isakeit, T.; Nichols, R. L. Automatic Classification of Cotton Root Rot Disease Based on UAV Remote Sensing. *Remote Sens.*, **2020**, *12* (8). https://doi.org/10.3390/RS12081310.

[31] Naidu, R. A.; Perry, E. M.; Pierce, F. J.; Mekuria, T. The Potential of Spectral Reflectance Technique for the Detection of Grapevine Leafroll-Associated Virus-3 in Two Red-Berried Wine Grape Cultivars. *Comput. Electron. Agric.*, **2009**, *66* (1), 38–45. https://doi.org/10.1016/j.compag.2008.11.007.

[32] Albetis, J.; Duthoit, S.; Guttler, F.; Jacquin, A.; Goulard, M.; Poilvé, H.; Féret, J. B.; Dedieu, G. Detection of Flavescence Dorée Grapevine Disease Using Unmanned Aerial Vehicle (UAV) Multispectral Imagery. *Remote Sens.*, **2017**, *9* (4), 1–20. https://doi.org/10.3390/rs9040308.

[33] Calderón, R.; Navas-Cortés, J. A.; Lucena, C.; Zarco-Tejada, P. J. High-Resolution Airborne Hyperspectral and Thermal Imagery for Early Detection of Verticillium Wilt of Olive Using Fluorescence, Temperature and Narrow-Band Spectral Indices. *Remote Sens. Environ.*, **2013**, *139*, 231–245. https://doi.org/10.1016/j.rse.2013.07.031.

[34] Mahlein, A. K.; Rumpf, T.; Welke, P.; Dehne, H. W.; Plümer, L.; Steiner, U.; Oerke, E. C. Development of Spectral Indices for Detecting and Identifying Plant Diseases. *Remote Sens. Environ.*, **2013**, *128*, 21–30. https://doi.org/10.1016/j.rse.2012.09.019.

[35] Nebiker, S.; Lack, N.; Abächerli, M.; Läderach, S. Light-Weight Multispectral Uav Sensors and Their Capabilities for Predicting Grain Yield and Detecting Plant Diseases. *Int. Arch. Photogramm. Remote Sens. Spat. Inf. Sci. - ISPRS Arch.*, **2016**, *2016-Janua*, 963–970. https://doi.org/10.5194/isprsarchives-XLI-B1-963-2016.

[36] Di, S. F.; Battiston, E.; Marco, S. D. I.; Matese, A.; Nocentini, M.; Palliotti, A.; Mugnai, L.; Gennaro, S. F. D. I.; Battiston, E.; Marco, S. D. I.; et al. Unmanned Aerial Vehicle (UAV) -Based Remote Sensing to Monitor Grapevine Leaf Stripe Disease within a Vineyard Affected by Esca Complex Union Stable URL : Https://Www.Jstor.Org/Stable/44809332 Unmanned

Aerial Vehicle (UAV) -Based Remote Sensing to Mon. **2020**.

[37] Zapolska, A.; Kalaitzidis, C.; Markakis, E.; Ligoxigakis, E.; Koubouris, G. Linear Discriminant Analysis of Spectral Measurements for Discrimination between Healthy and Diseased Trees of Olea Europaea L. Artificially Infected by Fomitiporia Mediterranea. *Int. J. Remote Sens.*, **2020**, *41* (14), 5388–5398. https://doi.org/10.1080/01431161.2020.1731931.

[38] Wu, M.; Yang, C.; Song, X.; Hoffmann, W. C.; Huang, W.; Niu, Z.; Wang, C.; Li, W.; Yu, B. Monitoring Cotton Root Rot by Synthetic Sentinel-2 NDVI Time Series Using Improved Spatial and Temporal Data Fusion. *Sci. Rep.*, **2018**, *8* (1), 1–12. https://doi.org/10.1038/s41598-018-20156-z.

[39] Huang, J.; Apan, A. Detection of Sclerotinia Rot Disease on Celery Using Hyperspectral Data and Partial Least Squares Regression. *J. Spat. Sci.*, **2006**, *51* (2), 129–142. https://doi.org/10.1080/14498596.2006.9635087.

[40] Huang, J.; Schmidt, A.; Gleixner, G.; Trumbore, S.; Hartmann, H. Co Sc. **2020**, 1–56.

[41] Trento province. *Provincia Autonoma Di Trento*; 2020.

[42] Junges, A. H.; Almança, M. A. K.; Fajardo, T. V. M.; Ducati, J. R. Leaf Hyperspectral Reflectance as a Potential Tool to Detect Diseases Associated with Vineyard Decline. *Trop. Plant Pathol.*, **2020**, *45* (5), 522–533. https://doi.org/10.1007/s40858-020-00387-0.

[43] Pertot, I.; Gobbin, D.; De Luca, F.; Prodorutti, D. Methods of Assessing the Incidence of Armillaria Root Rot across Viticultural Areas and the Pathogen's Genetic Diversity and Spatial-Temporal Pattern in Northern Italy. *Crop Prot.*, **2008**, *27* (7), 1061–1070. https://doi.org/10.1016/j.cropro.2007.12.013.

[44] Alt, V. V.; Gurova, T. A.; Elkin, O. V.; Klimenko, D. N.; Maximov, L. V.; Pestunov, I. A.; Dubrovskaya, O. A.; Genaev, M. A.; Erst, T. V.; Genaev, K. A.; et al. The Use of Specim IQ, a Hyperspectral Camera, for Plant Analysis. *Vavilovskii Zhurnal Genet. Selektsii*, **2020**, *24* (3), 259–266. https://doi.org/10.18699/VJ19.587.

[45] Barreto, A.; Paulus, S.; Varrelmann, M.; Mahlein, A. K. Hyperspectral Imaging of Symptoms Induced by Rhizoctonia Solani in Sugar Beet: Comparison of Input Data and Different Machine Learning Algorithms. *J. Plant Dis. Prot.*, **2020**, *127* (4), 441–451. https://doi.org/10.1007/s41348-020-00344-8.

[46] Lichtenthaler, H. K. Vegetation Stress: An Introduction to the Stress Concept in Plants. *J. Plant Physiol.*, **1996**, *148* (1–2), 4–14. https://doi.org/10.1016/s0176-1617(96)80287-2.

[47] Peñuelas, J.; Gamon, J. A.; Fredeen, A. L.; Merino, J.; Field, C. B. Reflectance Indices Associated with Physiological Changes in Nitrogen- and Water-Limited Sunflower Leaves. *Remote Sens. Environ.*, **1994**, *48* (2), 135–146. https://doi.org/10.1016/0034-4257(94)90136-8.

[48] Steele, M. R.; Gitelson, A. A.; Rundquist, D. C.; Merzlyak, M. N. Nondestructive Estimation of Anthocyanin Content in Grapevine Leaves. *Am. J. Enol. Vitic.*, **2009**, *60* (1), 87–92.

[49] Gitelson, A. A.; Keydan, G. P.; Merzlyak, M. N. Three-Band Model for Noninvasive Estimation of Chlorophyll, Carotenoids, and Anthocyanin Contents in Higher Plant Leaves. *Geophys. Res. Lett.*, **2006**, *33* (11), 2–6. https://doi.org/10.1029/2006GL026457.

[50] Singh, D.; Singh, S. Geospatial Modeling of Canopy Chlorophyll Content Using High Spectral Resolution Satellite Data in Himalayan Forests. *Clim. Chang. Environ. Sustain.*, **2018**, *6* (1), 20. https://doi.org/10.5958/2320-642x.2018.00003.0.

[51] Vogelmann, J. E.; Rock, B. N.; Moss, D. M. Red Edge Spectral Measurements from Sugar Maple Leaves. *Int. J. Remote Sens.*, **1993**, *14* (8), 1563–1575. https://doi.org/10.1080/01431169308953986.

[52] Pu, R.; Gong, P.; Yu, Q. Comparative Analysis of EO-1 ALI and Hyperion, and Landsat ETM+ Data for Mapping Forest Crown Closure and Leaf Area Index. *Sensors*, **2008**, *8* (6), 3744–3766. https://doi.org/10.3390/s8063744.

[53] Main, R.; Cho, M. A.; Mathieu, R.; O'Kennedy, M. M.; Ramoelo, A.; Koch, S. An Investigation into Robust Spectral Indices for Leaf Chlorophyll Estimation. *ISPRS J. Photogramm. Remote Sens.*, **2011**, *66* (6), 751–761. https://doi.org/10.1016/j.isprsjprs.2011.08.001.

[54] Bannari, A.; Morin, D.; Bonn, F.; Huete, A. R. A Review of Vegetation Indices. *Remote Sens. Rev.*, **1995**, *13* (1–2), 95–120.

https://doi.org/10.1080/02757259509532298.

[55] Gitelson, A. A.; Kaufman, Y. J.; Merzlyak, M. N. Use of a Green Channel in Remote Sensing of Global Vegetation from EOS- MODIS. *Remote Sens. Environ.*, **1996**, *58* (3), 289–298. https://doi.org/10.1016/S0034-4257(96)00072-7.

[56] Wu, W. The Generalized Difference Vegetation Index (GDVI) for Dryland Characterization. *Remote Sens.*, **2014**, *6* (2), 1211–1233. https://doi.org/10.3390/rs6021211.

[57] Carter, G. A. Ratios of Leaf Reflectances in Narrow Wavebands as Indicators of Plant Stress. *Int. J. Remote Sens.*, **1994**, *15* (3), 517–520. https://doi.org/10.1080/01431169408954109.

[58] Manevski, K.; Jabloun, M.; Gupta, M.; Kalaitzidis, C. *Field-Scale Sensitivity of Vegetation Discrimination to Hyperspectral Reflectance and Coupled Statistics*; Elsevier Inc., 2017. https://doi.org/10.1016/B978-0-12-803011-0.00006-9.

[59] Avola, G.; Di Gennaro, S. F.; Cantini, C.; Riggi, E.; Muratore, F.; Tornambè, C.; Matese, A. Remotely Sensed Vegetation Indices to Discriminate Field-Grown Olive Cultivars. *Remote Sens.*, **2019**, *11* (10). https://doi.org/10.3390/rs11101242.

[60] Kong, W.; Zhang, C.; Huang, W.; Liu, F.; He, Y. Application of Hyperspectral Imaging to Detect Sclerotinia Sclerotiorum on Oilseed Rape Stems. *Sensors (Switzerland)*, **2018**, *18* (1), 1–16. https://doi.org/10.3390/s18010123.

[61] Morel, J.; Jay, S.; Féret, J. B.; Bakache, A.; Bendoula, R.; Carreel, F.; Gorretta, N. Exploring the Potential of PROCOSINE and Close-Range Hyperspectral Imaging to Study the Effects of Fungal Diseases on Leaf Physiology. *Sci. Rep.*, **2018**, *8* (1), 1–13. https://doi.org/10.1038/s41598-018-34429-0.

[62] Chan, A. H. Y.; Barnes, C.; Swinfield, T.; Coomes, D. A. Monitoring Ash Dieback (Hymenoscyphus Fraxineus) in British Forests Using Hyperspectral Remote Sensing. *Remote Sens. Ecol. Conserv.*, **2020**, 1–15. https://doi.org/10.1002/rse2.190.

[63] Garhwal, A. S.; Pullanagari, R. R.; Li, M.; Reis, M. M.; Archer, R. Hyperspectral Imaging for Identification of Zebra Chip Disease in Potatoes. *Biosyst. Eng.*, **2020**, *197*, 306–317. https://doi.org/10.1016/j.biosystemseng.2020.07.005.

[64] Zhang, M.; Qin, Z.; Liu, X. Remote Sensed Spectral Imagery to Detect Late Blight in Field Tomatoes. *Precis. Agric.*, **2005**, *6* (6), 489–508. https://doi.org/10.1007/s11119-005-5640-x.

[65] Vescovo, L.; Wohlfahrt, G.; Balzarolo, M.; Pilloni, S.; Sottocornola, M.; Rodeghiero, M.; Gianelle, D. New Spectral Vegetation Indices Based on the Near-Infrared Shoulder Wavelengths for Remote Detection of Grassland Phytomass. *Int. J. Remote Sens.*, **2012**, *33* (7), 2178–2195. https://doi.org/10.1080/01431161.2011.607195.

[66] Liu, L. yun; Huang, W. jiang; Pu, R. liang; Wang, J. hua. Detection of Internal Leaf Structure Deterioration Using a New Spectral Ratio Index in the Near-Infrared Shoulder Region. *J. Integr. Agric.*, **2014**, *13* (4), 760–769. https://doi.org/10.1016/S2095-3119(13)60385-8.

[67] Gausman, H. W. Leaf Reflectance of Near-Infrared. *Photogramm Eng*, **1974**, *40* (2), 183–191.

[68] Reynolds, G. J.; Windels, C. E.; MacRae, I. V.; Laguette, S. Remote Sensing for Assessing Rhizoctonia Crown and Root Rot Severity in Sugar Beet. *Plant Dis.*, **2012**, *96* (4), 497–505. https://doi.org/10.1094/PDIS-11-10-0831.

[69] Imran, H. A.; Gianelle, D.; Rocchini, D.; Dalponte, M.; Martín, M. P.; Sakowska, K.; Wohlfahrt, G.; Vescovo, L. VIS-NIR, Red-Edge and NIR-Shoulder Based Normalized Vegetation Indices Response to Co-Varying Leaf and Canopy Structural Traits in Heterogeneous Grasslands. *Remote Sens.*, **2020**, *12* (14). https://doi.org/10.3390/rs12142254.

[70] Nogales, A.; Aguirreolea, J.; Santa María, E.; Camprubí, A.; Calvet, C. Response of Mycorrhizal Grapevine to Armillaria Mellea Inoculation: Disease Development and Polyamines. *Plant Soil*, **2009**, *317* (1–2), 177–187. https://doi.org/10.1007/s11104-008-9799-6.

[71] Pérez-Bueno, M. L.; Pineda, M.; Vida, C.; Fernández-Ortuño, D.; Torés, J. A.; de Vicente, A.; Cazorla, F. M.; Barón, M. Detection of White Root Rot in Avocado Trees by Remote Sensing. *Plant Dis.*, **2019**, *103* (6), 1119–1125. https://doi.org/10.1094/PDIS-10-18-1778-RE.

[72] Granum, E.; Pérez-Bueno, M. L.; Calderón, C. E.; Ramos, C.; de Vicente, A.; Cazorla, F. M.; Barón, M. Metabolic Responses of Avocado Plants to Stress Induced by Rosellinia Necatrix Analysed by Fluorescence and Thermal Imaging. *Eur. J. Plant Pathol.*, **2015**, *142* (3), 625–632. https://doi.org/10.1007/s10658-015-0640-9.

[73] Mahlein, A.-K.; Kuska, M. T.; Behmann, J.; Polder, G.; Walter, A. Hyperspectral Sensors and Imaging Technologies in Phytopathology: State of the Art. *Annu. Rev. Phytopathol.*, **2018**, *56* (1), 535–558. https://doi.org/10.1146/annurev-phyto-080417-050100.

[74] Mutanga, O.; Skidmore, A. K. Red Edge Shift and Biochemical Content in Grass Canopies. *ISPRS J. Photogramm. Remote Sens.*, **2007**, *62* (1), 34–42. https://doi.org/10.1016/j.isprsjprs.2007.02.001.

[75] Steele, M.; Gitelson, A. A.; Rundquist, D. Nondestructive Estimation of Leaf Chlorophyll Content in Grapes. *Am. J. Enol. Vitic.*, **2008**, *59* (3), 299–305.

[76] Pinar, A.; Curran, P. J. Technical Note: Grass Chlorophyll and the Reflectance Red Edge. *Int. J. Remote Sens.*, **1996**, *17* (2), 351–357. https://doi.org/10.1080/01431169608949010.

[77] Camprubi, A.; Solari, J.; Bonini, P.; Garcia-Figueres, F.; Colosimo, F.; Cirino, V.; Lucini, L.; Calvet, C. Plant Performance and Metabolomic Profile of Loquat in Response to Mycorrhizal Inoculation, Armillaria Mellea and Their Interaction. *Agronomy*, **2020**, *10* (6), 1–13. https://doi.org/10.3390/agronomy10060899.

[78] Torrigiani, P.; Serafini-Fracassini, D.; Fara, A. Diamine Oxidase Activity in Different Physiological Stages of Helianthus Tuberosus Tuber. *Plant Physiol.*, **1989**, *89* (1), 69–73. https://doi.org/10.1104/pp.89.1.69.

[79] Heritage, C. Spectral Remote Sensing of Tomato Plants (Lycopersicon Esculentum L .) Infected with Tomato Mosaic Virus (ToMV). **2010**.

[80] Minocha, R.; Shortle, W. C.; Lawrence, G. B.; David, M. B.; Minocha, S. C. Relationships among Foliar Chemistry, Foliar Polyamines, and Soil Chemistry in Red Spruce Trees Growing across the Northeastern United States. *Plant Soil*, **1997**, *191* (1), 109–122. https://doi.org/10.1023/A:1004293523185.

[81] Vergara-Diaz, O.; Vatter, T.; Kefauver, S. C.; Obata, T.; Fernie, A. R.; Araus, J. L. Assessing Durum Wheat Ear and Leaf Metabolomes in the Field through Hyperspectral Data. *Plant J.*, **2020**, *102* (3), 615–630. https://doi.org/10.1111/tpj.14636.

[82] Candiago, S.; Remondino, F.; De Giglio, M.; Dubbini, M.; Gattelli, M. Evaluating Multispectral Images and Vegetation Indices for Precision Farming Applications from UAV Images. *Remote Sens.*, **2015**, *7* (4), 4026–4047. https://doi.org/10.3390/rs70404026.